minerals

MDPI

Article

Geochemical Dynamics and Evolutionary Implications of Sediments at the Xingu–Amazon Rivers' Confluence: Proxies for Mixing, Mobility and Weathering

Lucio Cardoso Medeiros Filho [1,2,*], Nils Edvin Asp [3], Jean Michel Lafon [4], Thiago Pereira Souza [5], José Francisco Berredo [6] and Gabriel Negreiros Salomão [2]

1 Program in Geology and Geochemistry, Institute of Geosciences, Federal University of Pará, Belém 66075-110, PA, Brazil
2 Vale Technological Institute, Rua Boaventura da Silva, 955, Belém 66055-090, PA, Brazil; gabriel.salomao@itv.org
3 Coastal Geology Laboratory, Institute for Coastal Studies, Federal University of Pará, Bragança, Belém 68600-000, PA, Brazil; nilsasp@ufpa.br
4 Isotopic Geology Laboratory, Institute of Geosciences, Federal University of Pará, Belém 66075-110, PA, Brazil; lafonjm@ufpa.br
5 Graduate Program in Geosciences, Institute of Geosciences, Federal University of Rio Grande do Sul, Porto Alegre 91501-970, RS, Brazil
6 Museu Paraense Emílio Goeldi, Coordination of Earth Sciences and Ecology (CCTE), Av. Perimetral 1901, Belém 66077-830, PA, Brazil; berredo@museu-goeldi.br
* Correspondence: lucio.filho@pq.itv.org

Abstract: This study investigates the geochemical characteristics and evolutionary implications of sediments at the confluence of the Xingu and Amazon Rivers. The main objective is to understand sediment mixing, mobility, and weathering processes through geochemical proxies. Samples were collected from various sections of the lower Xingu River, focusing on its interaction with the Amazon River. Analytical techniques such as X-ray diffraction (XRD), X-ray fluorescence (XRF), and inductively coupled plasma mass spectrometry (ICP-MS) were employed to analyze major and trace elements. The results reveal significant spatial variations in mineralogical and textural patterns, with sediments forming distinct groupings based on their location. The data suggest that the lower Xingu River is strongly influenced by sediment inputs from the Amazon River, particularly affecting sediment composition and chemical weathering processes. This research highlights the critical interactions between river systems and their implications for the evolution of the Amazon basin, especially regarding sediment contributions from various geological sources. Even though the Xingu River drains cratonic regions at higher elevations, the geochemistry of the bottom sediments confirms that the bedload is derived from heterogeneous sources with primarily intermediate igneous compositions and has undergone substantial recycling during river transport.

Keywords: geochemistry; weathering; provenance; sediment transport; Xingu River; Amazon River

Citation: Medeiros Filho, L.C.; Asp, N.E.; Lafon, J.M.; Souza, T.P.; Berredo, J.F.; Salomão, G.N. Geochemical Dynamics and Evolutionary Implications of Sediments at the Xingu–Amazon Rivers' Confluence: Proxies for Mixing, Mobility and Weathering. *Minerals* **2024**, *14*, 1101. https://doi.org/10.3390/min14111101

Academic Editor: Luca Aldega

Received: 31 August 2024
Revised: 16 October 2024
Accepted: 25 October 2024
Published: 29 October 2024

1. Introduction

The geochemical analysis of fluvial sediments is a valuable tool for studying the origin, hydrological conditions, paleoenvironmental reconstructions, and anthropogenic impacts on rivers. The chemical composition of river sediments is significantly influenced by source rocks, sedimentary recycling, and post-depositional modifications during diagenesis and metamorphism [1–3]. However, this analysis is challenging due to the complex interplay of these factors and their varying effects under different climatic conditions. As sediments are formed, transported, and deposited, they experience structural, mineralogical, and geochemical transformations. The observed variation, caused by the processes of weathering

and fractionation, adds complexity to the study of their source and the conditions of local hydrodynamics [3–7].

The Xingu River and other tributaries of the Lower sector in the Amazon basin originating from distinct geological formations converge at their mouth with more recent sediments from the Amazon River. Studies indicate that the headwaters of the Xingu River and the Amazon River contribute to the sediments in the broader section known as the ria. However, the extent of interaction between these two river systems is currently unknown [8–12]. An analysis of mixing proxies and elemental geochemistry is necessary to evaluate the influence of the main river on its tributaries by examining their signatures in order to comprehend the dynamics of the sediments and the hydrological conditions of these ecosystems. The investigation of these processes is essential for a comprehensive knowledge of the river systems of the region, as the influence of the tide brings variability that can have a significant impact on recent deposits.

While few investigations have examined the lower tributaries, the majority of geochemical studies on the Amazon River have concentrated on the central Amazon region, which encompasses around 30% of the 6 million km^2 drainage basin [13–16]. A comprehensive study has been conducted in the lower Amazon to examine the dispersion of geochemical and mineralogical components in both the primary channel and significant tributaries [14,17–19].

Nevertheless, the existing research has mostly concentrated on suspended matter, thereby posing difficulties in the study of blackwater and clearwater rivers, such as the Xingu River, owing to the limited quantity of suspended matter present. Existing research on bedload sediments or floodplains primarily focuses on the central region of the Amazon basin, particularly in the Solimões, Madeira, and, more recently, Tapajós rivers [10,15,16,20]. However, the tributaries in the lower part of the basin have received limited attention in research.

A post-glacial sea-level rise in the Amazon basin led to sediment deposition, obstructing lower tributaries such as the Xingu River and creating submerged valleys (rias) at their confluences. This was due to the tributaries originating in Proterozoic terrains being unable to transport enough sediment to fill their incised valleys [8,9,21]. In order to obtain a deeper comprehension of hydrological conditions, sediment sources, and weathering processes, this study will assess the capacity of geochemical markers to detect mixing and interaction among river systems of various origins. The important goals of this research include comprehending the evolution of river systems and assessing current effects in confluence zones like the Amazon and Xingu rivers [22,23].

Physiographic and Geological Settings

As a major tributary of the Amazon basin, the Xingu River originates in the Archean terrain of the Brazilian Shield, characterized by ancient crystalline rocks such as gneisses and granites. The geological characteristics of the upper course of the river influence its topography, resulting in a landscape marked by prominent mountain ranges and steep slopes. The Proterozoic geological units, which exert ongoing influence on the geomorphology and erosion processes, are traversed by the Xingu River over its northern trajectory [24–26].

Upon its descent, the Xingu River flows into the Amazon Sedimentary Basin (Figure 1), a vast area composed of younger and less consolidated sediments, including sandstones and claystone, that were created over millions of years. The environment in the region exhibits geological and biological complexity, characterized by alluvial plains, fertile soils, and meandering river channels. These features arise from the transition between ancient crystalline formations and more recent deposits.

The lower course of the Xingu River is located in the northern portion of the Central Amazonian Province [27,28], on the boundary between the sedimentary basin of the Amazon (Paleozoic to Neogene) and its basement composed of Mesoarchean to Paleoproterozoic units (Vasquez and Rosa-Costa). These units are mainly represented by charnockitoids and tonalitic orthogneisses, granodiorites, and granitoids of the Xingu Complex [24].

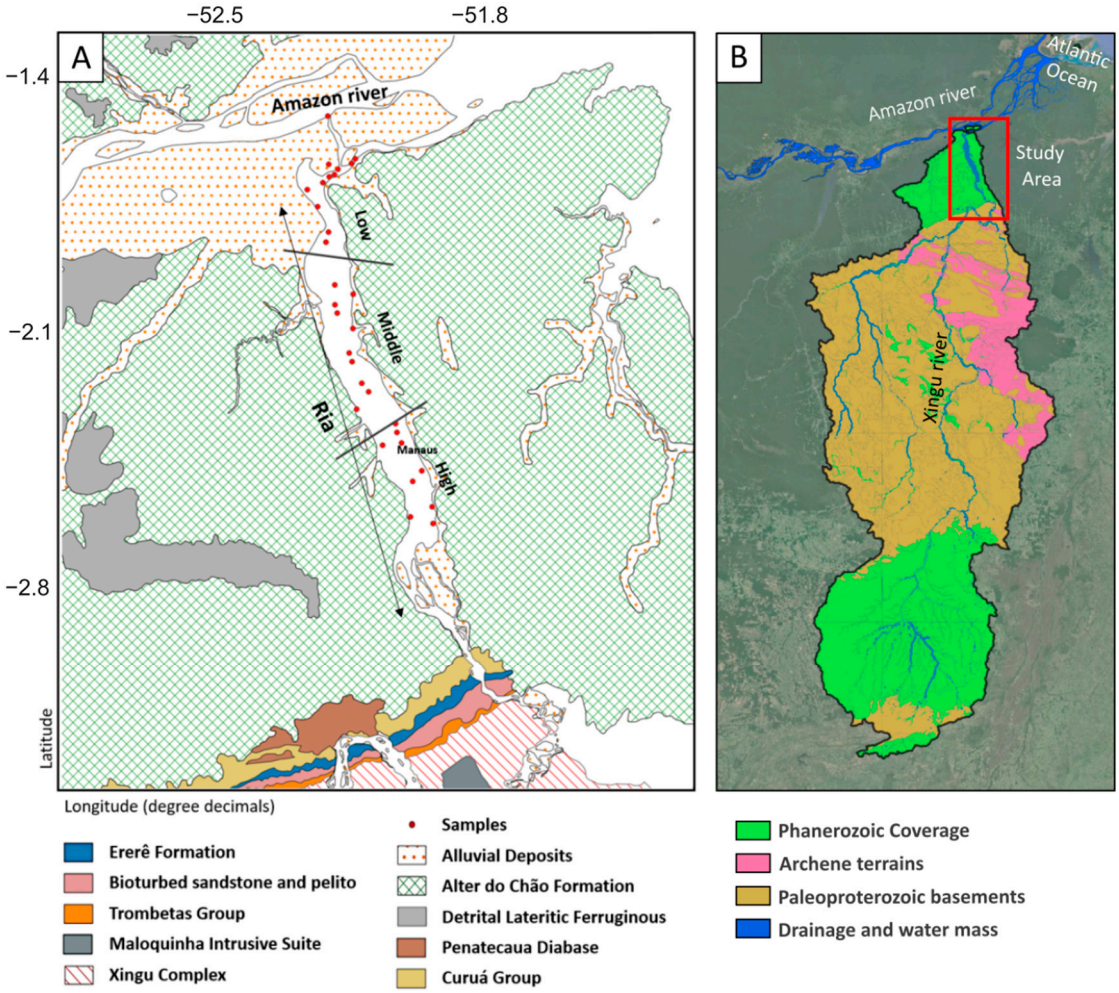

Figure 1. Location of the study area. The Xingu ria indicates the lower course of the basin and the region where it confluences with the Amazon River; the sampled points are divided into low, medium, and high sectors based on the local geology (**A**). The region the Xingu River basin occupies becomes the Amazon River before being emptied into the Atlantic Ocean (**B**).

2. Materials and Methods

2.1. Data Acquisition

The study involved the collection of bottom sediments during a specific time period (February 2016), and additional samples were taken in June 2018 to provide a detailed analysis of the Lower sector of the Xingu River and its confluence with the Amazon River.

Bottom sediments, in this context, are deposits that accumulate over time without significant seasonal effects and are useful in characterizing river environments with moderate hydrodynamics. Samples of bottom sediments were collected using a conventional Van Veen grab from a small aluminum boat, ensuring coverage of the entire study area. Navigation and positioning were conducted using a Garmin™ 60Map CSx GPS receiver (Lenexa, KS, USA).

2.2. Analytical Procedures

The percentages of sand, silt, and clay were determined using a laser diffraction granulometer, model Laser Diffraction SALD 2101 (Shimadzu (Kyoto, Japan)). The percentages of granulometric fractions, along with textural classification and statistics, were calculated for all samples following the methodology established by Folk and Ward (1957) [29].

The mineral compositions were determined through X-Ray Diffraction (XRD) analysis at the XRD Lab of the Geosciences Department of Federal University of Pará. A total of

32 samples were analyzed for major elements (SiO_2, Al_2O_3, Fe_2O_3, TiO_2, P_2O_5, MgO, CaO, Na_2O, and K_2O) and 30 trace elements (Ba, Ce, Cr, Cs, Dy, Er, Eu, Ga, Gd, Hf, Ho, La, Lu, Nb, Nd, Pr, Rb, Sm, Sn, Sr, Ta, Tb, Th, Tm, U, V, W, Y, Yb, and Zr). The samples were dried at 50 °C, disaggregated, sieved, and homogenized. Aliquots of 2 g were extracted from the total fraction (<2 mm) and digested with lithium metaborate or tetraborate. Quality control measures included the use of blanks and duplicates to ensure the accuracy and reliability of the results. X-Ray Fluorescence (XRF) and Inductively Coupled Plasma Mass Spectrometry (ICP-MS) were utilized to determine the major and trace elements, respectively, and gravimetric analysis was employed to examine the loss of ignition (LOI). ALS Global Analytical Laboratories conducted all sample analyses, with 28 used as a standard for sediment analysis. Details on the description of the analytical procedures are available at: http://www.alsglobal.com.

The relationships among the major elements were obtained through principal component analysis (PCA) using the XLSTAT® software (Trial Version 2021). accessed on 16 March 2022, considering other variables such as the location sector of the ria (1: Upper, 2: Middle, and 3: Lower), mineralogical group, and phi scale, the latter being obtained through granulometric analysis. Pearson correlations were used to determine elemental associations (major and trace elements, including REEs) in sediments. Highly significant correlations were identified based on critical values for the correlation coefficients at $p < 0.05$. Principal component analysis (PCA) was employed to explore relationships between variables and simplify data interpretation by identifying major controlling factors.

The major elements also allowed for the evaluation of the degree of chemical weathering based on the Chemical Index of Alteration (CIA), deduced by Nesbitt and Young (1986) [30], and the calculation of the molecular ratio of Al_2O_3-Na_2O + CaO-K_2O in the sediments. The results were plotted on an A-CN-K ternary diagram according to Fedo et al. 1995 and Nesbit and Young 1996 [31,32] to relate the influence of weathering on the compositional history of the sediments. The distribution of REEs in the sediments was used as a provenance indicator and to identify their relationship with the composition of potential source rocks.

3. Results

3.1. Mineralogical Groups and Textural Patterns

The Xingu River has traditionally been divided into three sectors: Upper, Middle, and Lower, to facilitate a more precise spatial interpretation of sediment distribution. In the central portion of the Xingu River (Upper and Middle sectors), a concordance was observed between mineralogical and granulometric data. Finer sediments were identified in the main river channel, accompanied by a diverse and homogeneous mineralogical assemblage, highlighting the presence of minerals such as kaolinite and anatase in the total fraction analyzed. Upstream, near the headwaters' delta, the same mineralogical assemblage was identified, though only discernible through the extraction of clay minerals.

A decrease in quartz abundance was noted in the central portion due to the predominance of finer sediments (silt + clay), which allowed for better discrimination of the constituent minerals. Despite the predominance of coarser grains in sample Amaz-18, it indicated that this sample originated from a sensitive zone that was beginning to differentiate from the upstream mineralogical assemblage (Figure 2).

Therefore, the mineralogical data evidenced certain geographical discrimination, which allowed for grouping by zones. Group 1 is associated with a high abundance of quartz-Qtz. The samples of this group are usually located near the shores, coinciding with the greater predominance of sand. In Group 2, it was possible to discriminate the presence of minerals such as kaolinite-Kln, quartz, and occasional occurrences of anatase-Ant and micas-Mca in areas located in the main channel of the ria. This group had the highest levels of occurrence, which extended throughout almost the entire study area. In Group 3, there is the occurrence of minerals such as smectite-Smc, micas-Mca, albite-Alb, and minor occurrences of kaolinite-Kln.

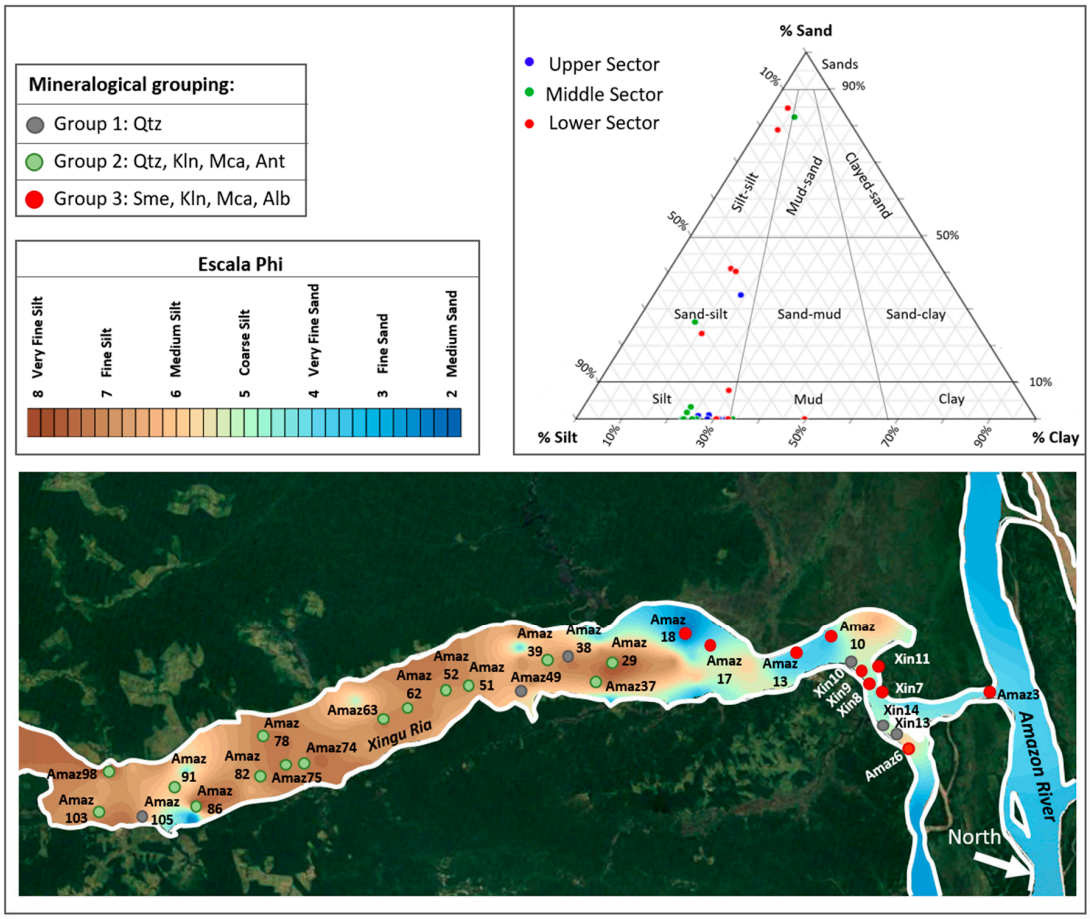

Figure 2. Categorization of recognized mineral assemblages and arrangement of granulometric samples in a triangular diagram based on the Sheppard classification (1959). One can undertake an interpolation of the granulometric classification based on the phi scale by using a larger sample size. An estimation of the granulometric classification based on the phi scale can be conducted in the research region by taking into account a larger sample size.

3.2. Oxide and Trace Geochemistry

The Al_2O_3 concentrations exhibited a relative decline from upstream to downstream, Fe_2O_3 displayed greater values in the Middle region, and CaO, MgO, Na_2O_3, and K_2O showed a substantial increase from upstream to downstream. The concentrations of TiO_2, P_2O_3, and BaO remained rather constant throughout sectors. High amounts of MnO were observed in certain samples within the Middle sector, as is evident in Table 1.

Table 1. Concentrations of major (weight % oxides) elements analyzed for the sediments by X-ray fluorescence (XRF).

	Sample	SiO_2	Al_2O_3	Fe_2O_3	CaO	MgO	Na_2O	K_2O	TiO2	MnO	P_2O_5	BaO	LOI	CIA
Upper Sector	AMAZ 103	46.6	22.9	7.62	0.26	0.39	0.09	1.06	0.78	0.09	0.22	0.07	21.8	94.20
	AMAZ 98	95.7	2.11	0.79	0.09	0.03	0.02	0.14	0.11	0.01	0.02	0.01	2.78	89.41
	AMAZ 105	97.2	0.73	1.06	0.04	<0.01	0.01	0.02	0.13	0.02	0.03	<0.01	1.65	91.25
	AMAZ 91	66.8	13.3	5.12	0.29	0.27	0.21	1.01	0.58	0.09	0.11	0.06	13.65	89.80
	AMAZ82	-	-	-	-	-	-	-	-	-	-	-	21.4	-
	AMAZ 78	47	21.3	7	0.23	0.37	0.1	1.04	0.71	0.14	0.18	0.07	21	93.96
	AMAZ 75	50	21.1	6.43	0.23	0.39	0.09	1.09	0.7	0.12	0.16	0.07	17.85	93.74
	AMAZ 74	48.6	20.9	7.87	0.27	0.38	0.09	0.99	0.68	0.16	0.18	0.07	20.7	93.93

Table 1. *Cont.*

	Sample	SiO_2	Al_2O_3	Fe_2O_3	CaO	MgO	Na_2O	K_2O	TiO2	MnO	P_2O_5	BaO	LOI	CIA
	Mean	64.5	14.62	5.1	0.20	0.31	0.09	0.76	0.53	0.09	0.13	0.06	15.10	92.33
	SD	22.9	9.54	3.0	0.10	0.14	0.07	0.47	0.28	0.06	0.08	0.02	8.39	2.11
	CV	35.4	65.24	58.6	48.00	46.63	75.17	61.48	53.94	63.51	60.65	41.17	55.57	2.29
Middle Sector	AMAZ 66	44	23.9	7.51	0.29	0.31	0.07	0.84	0.84	0.11	0.22	0.06	20.2	95.22
	AMAZ 63	48.2	20.1	6.63	0.28	0.35	0.12	0.98	0.66	0.14	0.22	0.06	21	93.58
	AMAZ 62	46.8	22.3	6.56	0.29	0.36	0.09	1.01	0.72	0.11	0.19	0.07	20.1	94.13
	AMAZ 52	46.9	23.1	7.39	0.18	0.37	0.08	1.03	0.71	0.17	0.26	0.07	20.3	94.71
	AMAZ 51	46.3	22.7	7.44	0.16	0.37	0.07	0.96	0.67	0.17	0.26	0.06	20.4	95.02
	AMAZ 49	74.1	9.55	3.48	0.11	0.13	0.05	0.36	0.82	0.04	0.09	0.03	10.25	94.84
	AMAZ 39	45.2	22.3	8.2	0.13	0.35	0.07	0.91	0.62	0.24	0.22	0.06	20.4	95.26
	AMAZ 38	44.7	22.3	8.92	0.12	0.37	0.08	0.91	0.64	0.26	0.23	0.05	20.6	95.26
	AMAZ 37	84.3	1.93	10.7	0.04	0.04	0.03	0.11	0.24	0.04	0.08	0.01	4.13	91.47
	AMAZ 29	45.8	21.3	8.27	0.19	0.42	0.1	0.92	0.61	0.24	0.19	0.06	20.6	94.62
	Mean	52.6	18.9	7.5	0.18	0.31	0.08	0.80	0.65	0.15	0.19	0.05	17.80	94.41
	SD	14.2	7.26	1.8	0.09	0.12	0.03	0.31	0.16	0.08	0.06	0.02	5.78	1.16
	CV	27.1	38.1	24.7	47.6	39.7	32.9	38.6	25.2	52.1	32.2	35.63	32.47	1.23
Lower Sector	AMAZ 18	62.3	11.85	11	0.63	0.69	0.72	1.36	0.57	0.15	0.17	0.07	10.55	81.39
	AMAZ 17	66	13.5	5.21	0.71	0.93	0.97	1.88	0.8	0.07	0.13	0.06	9.04	79.13
	AMAZ 13	74.7	10.2	4.01	0.61	0.64	0.99	1.64	0.59	0.04	0.07	0.05	6.34	75.89
	AMAZ 10	60.2	14.65	7.44	0.75	0.97	0.81	1.87	0.78	0.09	0.12	0.06	11.5	81.03
	XIN 10	88.7	4.92	2.07	0.5	0.34	0.39	0.73	0.33	0.04	0.06	0.03	3.64	75.23
	XIN 09	73.7	11.1	4.17	0.87	0.96	1.17	1.84	0.71	0.07	0.1	0.05	5.23	74.10
	XIN 08	67.9	13.15	5.02	0.9	1.16	1.11	2.13	0.84	0.08	0.13	0.06	6.61	76.06
	XIN 11	67.7	12.8	4.89	0.98	1.13	1.11	2.07	0.77	0.07	0.13	0.05	7.56	75.47
	XIN 14	98.2	0.5	0.85	<0.01	<0.01	0.02	0.14	0.03	0.01	0.03	<0.01	0.82	-
	XIN 13	96.7	1.51	1.07	0.13	0.09	0.21	0.31	0.12	0.01	0.03	0.01	0.93	69.91
	AMAZ 3	71.7	11.6	4.11	0.91	1	1	1.9	0.69	0.07	0.11	0.05	6.02	75.28
	Mean	75.2	9.6	4.5	0.70	0.79	0.77	1.44	0.57	0.06	0.10	0.05	6.20	76.35
	SD	13.3	4.9	2.9	0.25	0.35	0.39	0.72	0.28	0.04	0.05	0.02	3.48	3.42
	CV	17.7	51.5	63.7	36.1	44.25	51.0	49.70	49.81	61.78	45.96	35.28	56.16	4.47

The predominant components in oxide form were intricately linked to the silicon content. Al_2O_3, Fe_2O_3, and TiO_2 had negative correlations of 0.97, 0.62, and 0.61, correspondingly suggesting that a rise in silicon content resulted in a decrease in the abundance of these components. In contrast, CaO, MgO, and Na_2O did not exhibit a significant association. Nevertheless, it was feasible to distinguish their concentration zoning, suggesting that the Lower sector contained greater concentrations of these oxides (Figure 3).

A high negative correlation between Al_2O_3 and SiO_2 in river bottom sediments may indicate mineralogical separation between quartz and clay minerals, suggesting chemically mature sediments where quartz is predominant. This pattern may reflect differential weathering, with the removal of aluminum-rich minerals and the preservation of quartz, as well as influences from multiple sediment sources with distinct compositions. Textural variation may also play a role, with finer fractions enriched in Al_2O_3 and coarser fractions dominated by SiO_2 associated with depositional processes that segregate minerals based on their grain size and resistance to weathering.

The trace elements Ba, Cr, Ga, Hf, Nb, Rb, Sr, Ta, Th, U, V, W, Y, and Zr did not show significant variations along the extent of the ria; therefore, there were no geographic fluctuations in the contents of these elements (Table 2). Samples with high sand contents presented low concentrations of the mentioned elements, except for Zr and Hf, which had their highest concentrations in sandy samples with a predominance of quartz in their composition.

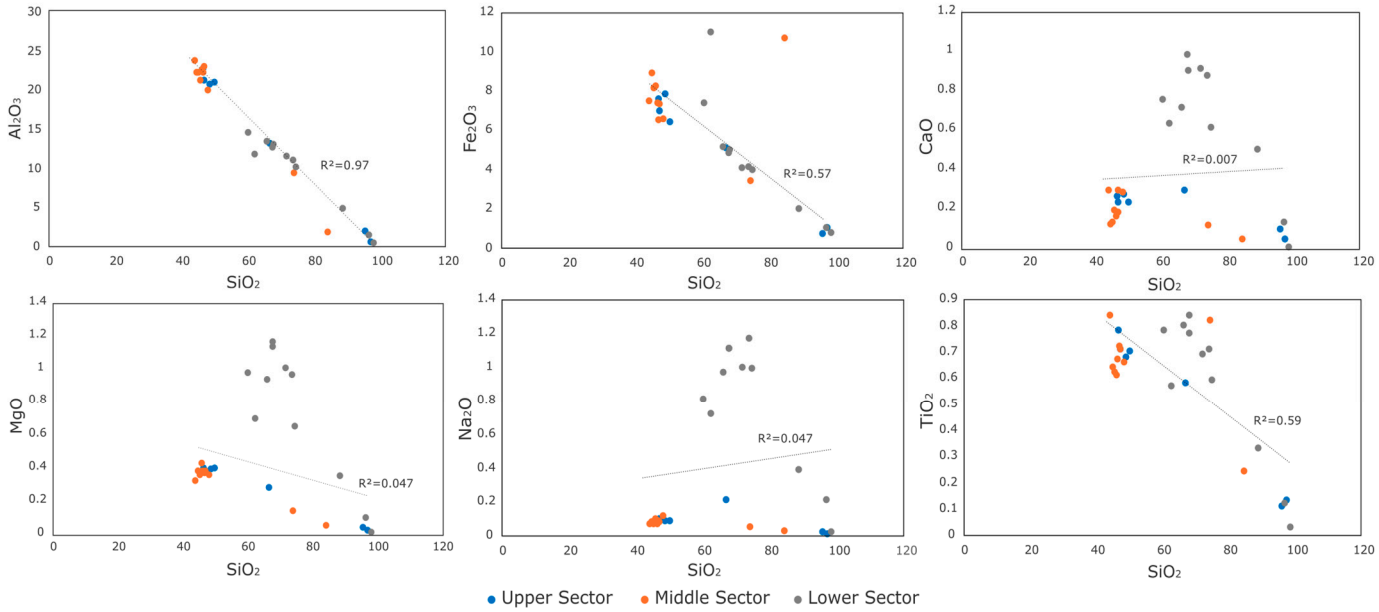

Figure 3. The main major oxides (wt%) in relation to silica (SiO_2) concentration are divided into sectors within the study area.

Table 2. Concentration of some trace elements. Additional information is available in the Supplementary Materials (Table S1).

Sample	Ba	Cr	Ga	Hf	Nb	Rb	Sn	Sr	Ta	Th	U	V	Y	Zr
AMAZ 103	610	80	29.6	5.9	17.3	70.5	3	45.6	1.1	22.9	4.23	67	36.7	225
AMAZ 98	109	10	4.1	4.4	4.1	10.2	1	12.6	0.1	5.14	1.08	13	6.9	171
AMAZ 105	44.7	10	1.6	2.9	3.3	2.3	<1	4.2	<0.1	3.11	0.75	9	4	104
AMAZ 91	518	110	23.2	14.6	15	59.2	2	52.9	1.1	17.4	3.72	73	30.2	576
AMAZ 82	710	80	30.2	6.1	17.2	71.9	4	60.2	1.2	24	4.52	71	35.9	226
AMAZ 78	556	60	25.9	5.3	16.9	59.4	3	41.1	1.1	21	3.71	63	32.8	200
AMAZ 75	637	70	28.3	6.5	17.3	68.2	3	47.6	1.2	22.5	3.77	64	36.3	240
AMAZ 74	781	80	30.8	6.6	17.7	71.8	4	52.8	1.1	24.8	4.59	71	38.1	244
Mean	496	62.5	21.71	6.54	13.60	51.69	2.86	39.63	0.99	17.61	3.30	53.88	27.61	248.25
SD	271.88	35.36	11.92	3.48	6.17	28.58	1.07	20.21	0.39	8.63	1.51	26.71	13.92	140.23
CV	54.85	56.57	54.90	53.28	45.36	55.29	37.42	51.01	39.91	49.03	45.89	49.58	50.42	56.49
AMAZ 66	445	60	26.3	6.4	16.6	47.3	2	38.7	1.2	20.8	3.38	68	27.8	232
AMAZ 63	485	60	24.3	4.6	14.2	54.2	2	40.3	1	19.8	3.63	57	29.9	179
AMAZ 62	600	70	29.1	5.3	16.5	64.3	4	44.1	1.1	21.8	3.75	68	34.4	198
AMAZ 52	625	120	34.7	5.3	17.1	74.5	3	44.3	1.2	24.3	4.06	95	34.9	190
AMAZ 51	659	90	34	5.3	17.2	75.2	4	43.6	1.1	24.4	4.26	82	37.4	189
AMAZ 49	276	80	14.4	20.2	19.7	26	2	24.8	1.3	17.9	3.91	48	27.8	798
AMAZ 39	446	60	25	3.5	11.6	52.6	3	28.3	0.9	18.1	2.94	67	26	129
AMAZ 38	494	70	29.1	3.9	13.4	62	3	34.3	0.8	20.4	3.52	75	28.2	141
AMAZ 37	81.9	30	4.2	9.7	5.2	8.1	1	9.6	0.2	5.47	1.67	79	17.9	394
AMAZ 29	549	70	28.9	3.9	14	65.3	3	43.8	0.8	21.3	3.63	78	30.8	147
Mean	466.09	71	24.24	5.83	10.87	40.35	2.7	29.23	0.7	15.72	2.94	71.7	25.725	259.7
SD	174.16	23.31	11.65	3.35	4.92	27.91	0.95	17.65	0.35	8.89	1.10	13.25	5.57	203.48
CV	37.37	32.83	48.06	57.41	45.25	69.17	35.14	60.39	49.49	56.55	37.46	18.48	21.67	78.35
AMAZ 18	746	50	18.9	8.3	12.9	69.1	2	119.5	0.7	13	2.64	95	30.4	315
AMAZ 17	456	30	14.7	8.7	13.8	64.6	2	105	0.9	10.15	2.63	72	26.8	339
AMAZ 13	522	40	15	9	13	73.4	2	131.5	0.7	10.05	2.54	66	26.7	342
AMAZ 10	625	60	21.7	7.9	18.3	104	3	140	1.1	14.45	3.51	105	36.1	306
XIN 10	252	50	7.2	6.9	8.2	34.7	2	63.7	0.5	5.31	1.63	33	15.7	257
XIN 09	479	70	14	10.7	15.8	82.6	3	161	1.1	10.55	2.68	68	30.6	421

Table 2. *Cont.*

Sample	Ba	Cr	Ga	Hf	Nb	Rb	Sn	Sr	Ta	Th	U	V	Y	Zr
XIN 08	512	80	16.8	13.7	18.5	96.8	3	163.5	1.4	12.45	3.66	92	36.7	525
XIN 11	511	80	15.4	10.2	17.9	94.7	4	166.5	1.3	11.9	3.21	88	36.3	360
XIN 14	45.1	20	1.7	1.4	1.1	4.6	1	3.9	0.1	1.8	0.53	<5	3.3	44
XIN 13	79.8	30	3.7	3.4	2.9	12.2	1	25.4	0.1	3.28	0.84	14	6.4	136
AMAZ 3	524	50	17.9	10.4	15.9	92.6	3	168	0.9	11.5	3.06	86	30.4	404
Mean	431.99	50.91	13.36	8.24	12.57	66.30	2.36	113.45	0.80	9.49	2.45	71.90	25.40	313.55
SD	217.71	20.23	6.40	3.42	6.03	34.51	0.92	58.24	0.44	4.15	1.03	28.69	11.77	132.47
CV	50.40	39.73	47.85	41.58	47.98	52.05	39.11	51.34	54.49	43.75	42.09	39.90	46.34	42.25

3.3. Rare Earth Elements and Normalization

No substantial variations were seen in the quantities of Rare Earth Elements (REEs) along the ria; the table with REE concentrations can be found in the Supplementary Materials (Table S1). Nevertheless, when we removed the samples from the river edges characterized by a significant amount of sand and minimal sequestration of rare earth elements (REEs), there was a noticeable decline in the values of HREEs in the upstream–downstream direction. With an average of 331.5 mg·kg^{-1}, the Upper sector had the highest HREE concentrations (253.5–372.7 mg·kg^{-1}), followed by the Middle sector (153.8–353.1 mg·kg^{-1}) with an average of 287.8 mg·kg^{-1}, and the Lower sector (168.3–257.1 mg·kg^{-1}), with an average of 201.5 mg·kg^{-1}. All sectors exhibited relative enrichment in comparison to the Upper Continental Crust (UCC), with the exception of sandy samples in the Middle and Upper sectors (Figure 4). The rare earth elements (REEs) were conventionally categorized as Light Rare Earth Elements (LREE, La to Eu) and Heavy Rare Earth Elements (HREE, Gd to Lu). LREE, particularly La and Ce, were more prevalent than HREE. The high positive correlation (r = 0.91) between Al_2O_3 and HREE suggests they are mainly associated with Al-silicate fractions, typically clay.

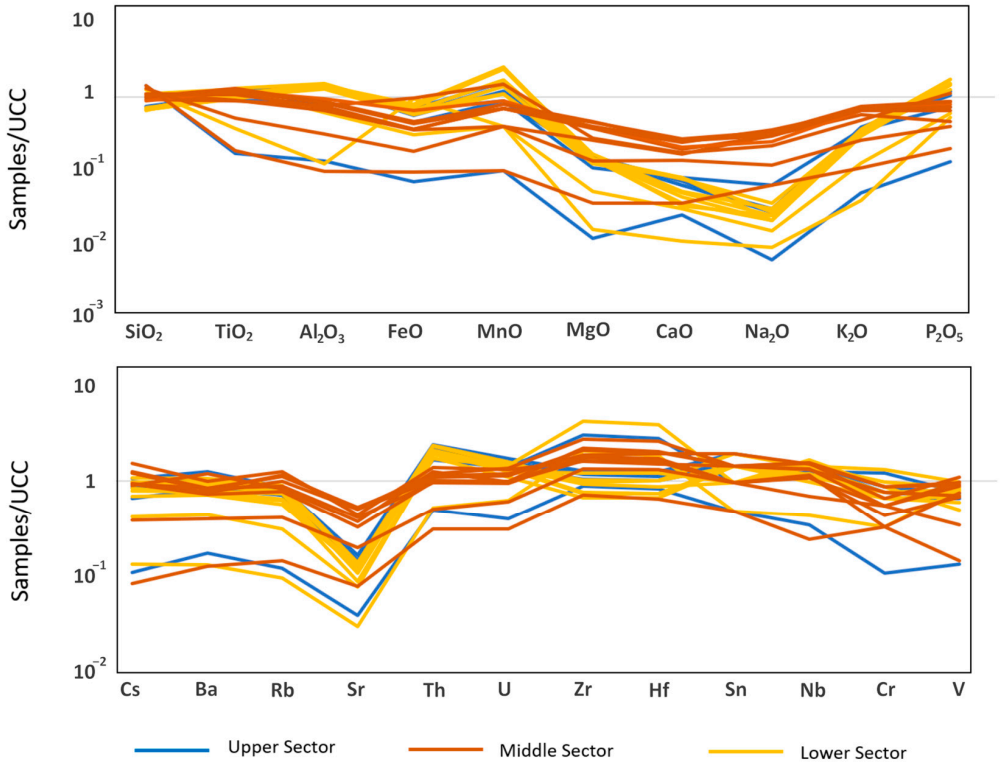

Figure 4. Major oxide and trace element normalization to the Upper Continental Crust (UCC) and color-coded sectorization.

3.4. Principal Component Analysis (PCA)

One approach to elucidate pathways for geochemical interpretation of sediments in the Xingu River involved Principal Component Analysis (PCA). For major elements, the two principal components (PC) (Figure 5) collectively accounted for 80.72% (F1: 42.17%; F2: 38.55%) of the total variance, revealing a certain level of alignment between samples located in the Lower sector and elements such as CaO and Na_2O. However, samples from the Upper and Middle sectors were predominantly and strongly associated with Fe_2O_3, Al_2O_3, P_2O_5, MnO, and the phi scale to a lesser extent.

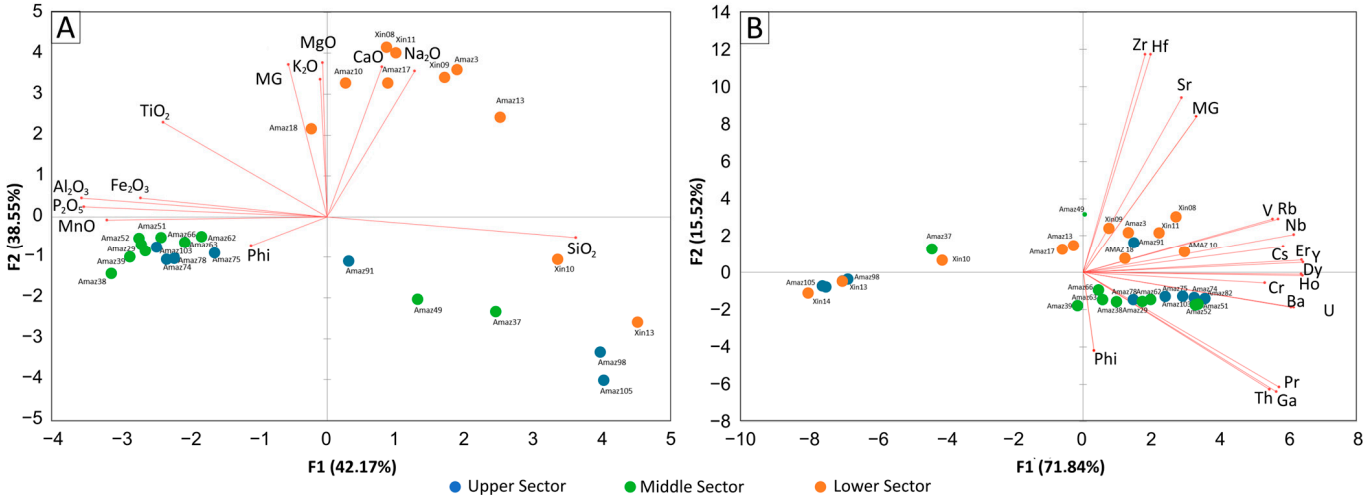

Figure 5. PCA analysis for major elements (**A**) trace elements (**B**). The analysis included the implementation of mineralogical groups (MG) and the phi scale. The correlation matrix is found in the Supplementary Material (Table S2).

Based on the weighting of each variable's contribution, there is a high positive load for SiO_2 and a high negative load for MnO, P_2O_3, Al_2O_3, Fe_2O_3, and, to a lesser extent, TiO_2 and the phi scale in F1. F2 is characterized by a high positive load for K_2O, MgO, CaO, Na_2O, and the mineralogical group. The actor analysis is found in the Supplementary Materials (Table S3).

Samples Amaz-105, Amaz-98, and Amaz-91 from the Upper sector, samples Amaz-49 and Amaz-37 from the Middle sector, and samples Xin-10 and Xin-13 from the Lower sector showed a certain degree of correlation with silicon content (Figure 5A). The PCA analysis effectively discriminated between two groups, the Lower sector and the Middle and Upper sectors, in terms of elemental geochemistry and other associated variables, such as the mineralogical group and the phi scale.

For trace elements, the two principal components (F1 and F2) collectively accounted for 87.36% (F1: 71.84%; F2: 15.52%) of the total variance.

Based on the weighting of each variable's contribution, there is a high positive load for V, Rb, Nb, Cs, Er, Y, Dy, Ho, Ba, Cr, and U in F1 (Figure 5B). F2 is characterized by a high positive load of Zr, Hf, location sector, and, to a lesser extent, Sr and the mineralogical group. Only the phi scale exhibits a negative load.

4. Discussion

4.1. Effects of Reworking Grain and the Amazon River

Based on textural and mineralogical characteristics as well as sediment geochemistry, a cluster of samples in the upstream areas (Upper and Middle sectors) has been mineralogically identified as Group 1 (Figure 2). The samples from this category consist mainly of quartz and exhibit varied textural patterning, mainly sand, suggesting limited sediment reworking. The results for these samples suggest a substantial influence from the banks, possibly by erosional action and predominance of quartz.

The main channel of the ria, representing the Middle sector, regardless of the method used, exhibited a finer textural pattern composed mainly of silt and clay. Associated mineralogy also indicated greater diversity and distinctive geochemistry in terms of elements associated with immobile ratios, suggesting more significant grain reworking.

Despite some mineralogical homogeneity, primarily marked by the presence of quartz often associated with feldspars; the more pronounced appearance of feldspars was limited to the Lower sector when compared to the Middle and Upper sectors, which exhibited peaks in samples located near the confluence with the Amazon River and little-to-none upstream. Samples from the Middle and Upper sectors were primarily marked by the presence of quartz, kaolinite, and anatase and the absence of feldspars, indicating a more mature and leached mineralogical assemblage compared to the downstream area. In the latter, the presence of feldspars and smectite suggests mineralogical immaturity.

In a thorough geochemical study of the Amazon River, covering a distance from its mouth to about 2500 km upstream, Martinelli et al. (1993) [13] found a significant decrease in the amount of quartz and a significant increase in the amounts of smectite/vermiculite downstream of the Xingu River confluence.

Mineli (2013) [33] and Souza (2018) [34] underscored significant disparities in the heavy mineral assemblage observed in the lower reaches of the Xingu River, attributing these differences to sediment input from varied origins. Their findings further revealed a pronounced presence of both tourmaline and zircon in the sand samples from the Volta Grande region (the research area's upstream) as well as the downstream portion of the Xingu River. This suggests a sedimentary source predominantly influenced by igneous rock contributions. In a multifaceted study employing mineralogical, geochemical, and isotopic signatures, Medeiros Filho et al. (2016) [20] delved into the hydrodynamic processes influencing recent bottom sediments in the lower stretches of the Tapajós River. The impact of the Amazon River on bottom sediment deposition and their subsequent mixing appeared to be restricted predominantly to the confluence region. Observations from the Xingu River mirrored this trend, thus proposing a consistent sedimentary deposition model for the lower tributaries of the Amazon.

Principal Component Analysis (PCA) further strengthens investigative techniques by using geochemical indicators of elemental ratios to distinguish the bottom sector well. A potential contribution of the Amazon River to the main channel of the Xingu River was suggested by the more pronounced separation observed in major elements (oxides). The samples from all sectors examined exhibited distinct divisions in the Lower sector (Amaz105, Amaz98, and Amaz91), Middle sector (Amaz49 and Amaz37), and Lower sector (Xin10, Xin13, and Xin14), segregated into discrete quadrants during the PCA analysis. The presented data support the mineralogical assemblages depicted in Figure 2. This collection of samples exhibits the greatest silica concentration and displays a granulometric composition of sandy material, suggesting a lower degree of sediment reworking.

4.2. Chemical Weathering

In a comprehensive geochemical analysis of the Amazon River, spanning from its mouth to nearly 2500 km upstream, Martinelli et al. (1993) [13] observed a marked decline in quartz abundance coupled with a notable rise in the smectite/vermiculite abundances downstream of the Xingu River confluence.

The composition of major elements in river sediments is utilized to estimate the chemical and physical weathering, to determine the relationships between elements and rock classifications, as well as to evaluate the geochemical processes operating in the river basin [35,36].

For the interpretation of the intensity of chemical weathering, proxies were applied, which tend to reflect the alteration of sediment particles. The K2O/Al2O3 ratio is commonly interpreted as a proxy for alteration because potassium is a water-soluble element released during the breakdown of K-feldspar and has been applied to the study of sediments in continental margins [37–39].

The K2O/Al2O3 ratio showed a negative correlation with SiO2/Al2O3, implying that sandier sediments are generally less altered than mud-rich sediments, suggesting formation processes between the Middle and Upper sectors of the lower ria (Figure 6).

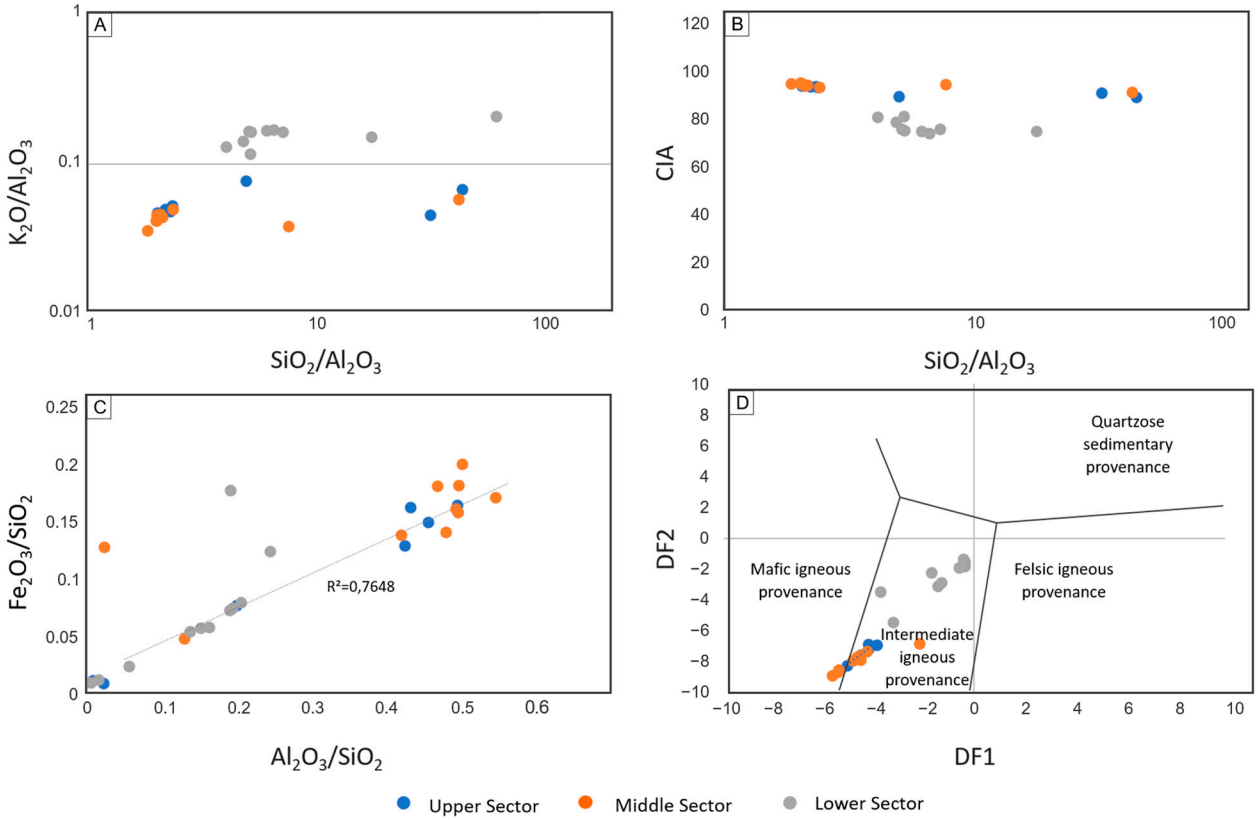

Figure 6. K_2O and SiO_2 normalized to Al_2O_3 (**A**), and CIA compared to SiO_2/Al_2O_3 indicate field separation (**B**). Fe_2O_3 and Al_2O_3 normalized to SiO_2 linearly separate the fields (**C**) as well as DF2 vs. DF1 diagrams, indicate source provenance (**D**). Roser and Korsch (1985) [40] proposed the use of discriminant functions (DF1 = 30.68 × TiO_2/Al_2O_3 − 12.54 × Fe_2O_3/Al_2O_3 + 7.33 × MgO/Al_2O_3 + 12.03 × Na_2O/Al_2O_3 + 35.40 × K_2O/Al_2O_3 − 6.38 e DF2 = 56.5 × TiO_2/Al_2O_3 − 10.88 × FeO_3 + 30.87 × MgO/Al_2O_3 − 5.40 × Na_2O/Al_2O_3 + 11.11 × K_2O/Al_2O_3 − 3.89) to divide the fields related to the different provenances of sedimentary rocks (source rocks: quartzose, intermediate, felsic, and mafic sedimentary).

If we consider a progressive increase in the K2O/Al2O3 ratio downstream, we can observe that the state of chemical weathering in the lower course of the Xingu River differs significantly from that in much of the main channel. Although sediments in the Upper and Middle sectors of the ria appear to be slightly more altered than those of the Lower sector, greater alteration may reflect slower transport times in the Upper sectors, with downstream sediment dilution due to a greater supply of fresher sources.

Nesbitt and Young (1982) [30] proposed the quantification of chemical weathering intensity expressed as a chemical index of alteration (CIA) using the formula:

$$CIA = [Al_2O_3/(Al_2O_3 + CaO^* + Na_2O + K_2O)] \times 100$$

A correction for CaO from carbonate contribution was not done, as CO_2 was not determined. So, to compute CaO*, the assumption proposed by McLennan (1993) [40] was adopted. After subtracting the amount of CaO due to apatite, CaO values were always greater than Na_2O; consequently, it was assumed that the concentration of CaO is equal to that of Na_2O. The CIA was developed for use in soil profiles, but its application has commonly been extended to river sediments and cores [36,39,41].

The CIA and K_2O/Al_2O_3 ratio highlighted the Lower sector (confluence) from the Middle and Upper sectors when crossed with the Si_2/Al_2O_3 ratio (Figure 6), although they show little correlation. It also distinguishes the Middle and Upper sectors from the Lower sector. There is clear evidence of a degree of correlation between the sample location, degree of alteration, or grain size. Additionally, grain size appears to be a primary control in the alteration proxy for understanding weathering in the system.

The Fe2O3/SiO2 vs. Al2O3/SiO2 plot (Figure 6) exhibited a strong correlation between the ratios, making it possible to discriminate two groups. One group primarily consisted of samples from the Lower sector, while the other group, mostly from the Middle and Upper sectors, indicated higher concentrations of clay minerals.

In the Roser and Korsch (1988) [40] provenance discrimination diagram, the discriminant functions formulated (i.e., bivariate) are based on concentrations of immobile major elements and variables. In this diagram (Figure 6D), the sediments from this study were situated in the field of intermediate igneous provenance, with some samples from the Middle sector suggesting a provenance from mafic igneous rocks, likely associated with the presence of metavolcanic sequences near Volta Grande upstream. However, the samples were essentially derived from mixed-source rocks.

The Xingu Complex presents a lithological diversity composed of mafic, felsic and intermediate rocks, such as amphibolites, metagabbros, granites, and gneisses. The erosion of these rocks upstream of the lower course of the Xingu River generates sediments with a rich mineralogical mixture, with mafic minerals such as pyroxenes and amphiboles, in addition to quartz and feldspar from felsic sources, resulting in deposits with intermediate igneous signatures. Downstream, the Amazon River increases the heterogeneity of the sediments by mixing materials brought from different geological regions. The Amazon contributes allochthonous sediments, which amplify the mineralogical and lithological diversity in the lower Xingu, combining mafic, felsic, and sedimentary sources and further enriching the composition of the deposits.

One way to assess chemical weathering was to plot the calculated Chemical Index of Alteration (CIA) for various samples within a triangular diagram (Figure 7). Another objective was to demonstrate how the Xingu River samples compare to the Upper Continental Crust (UCC, Taylor and McLennan 1985) [41], Average Post-Archean Australian Shale (PAAS, Taylor and McLennan 1985), and the average of established studies on the Amazon River [16,20]. The sediments in the Lower sector stand apart from the main river channel, showing lower CIA values, indicating lesser alteration. The Amazon River is a higher hydrodynamic environment, but its sediment originates from the Andes, covering a long path beneath Phanerozoic units. If its contribution to the Lower sector is confirmed, it would explain the presence of less altered sediments. This reduced state of alteration also reflects fast transport through floodplains, where most chemical weathering occurs.

According to Ahmad and Chandra (2013) [22], Figure 7 shows the computed CIA values for several samples in a triangle Al_2O_3-CaO + Na_2O-K_2O diagram and shows how the samples from the Xingu River relate to those from other significant rivers. Less-changed patterns are indicated by lower CIA scores. The trend suggests that the less-changed material is contributing to the main flow from other sources or that we are sampling progressively sandier material downstream.

The weathering index showed a progressive reduction downstream, with higher rates at the beginning of the ria and a decreasing trend as the Amazon River approaches. This situation demonstrates a natural recycling pattern. The results suggest that source rocks in the upper reaches may be more susceptible to chemical weathering compared to rocks present in the lower areas of the basin. As the river progresses, it may cross less weathered geological formations, such as the transition from the Xingu complex (Archean) to the Alter do Chão formation (Phanerozoic). This geological transition along the Xingu River is well marked by the diversity of landscapes, which vary from rocky escarpments and waterfalls in the Volta Grande of the Xingu River (upstream of the ria) to broad and fertile alluvial plains closer to the Amazon River.

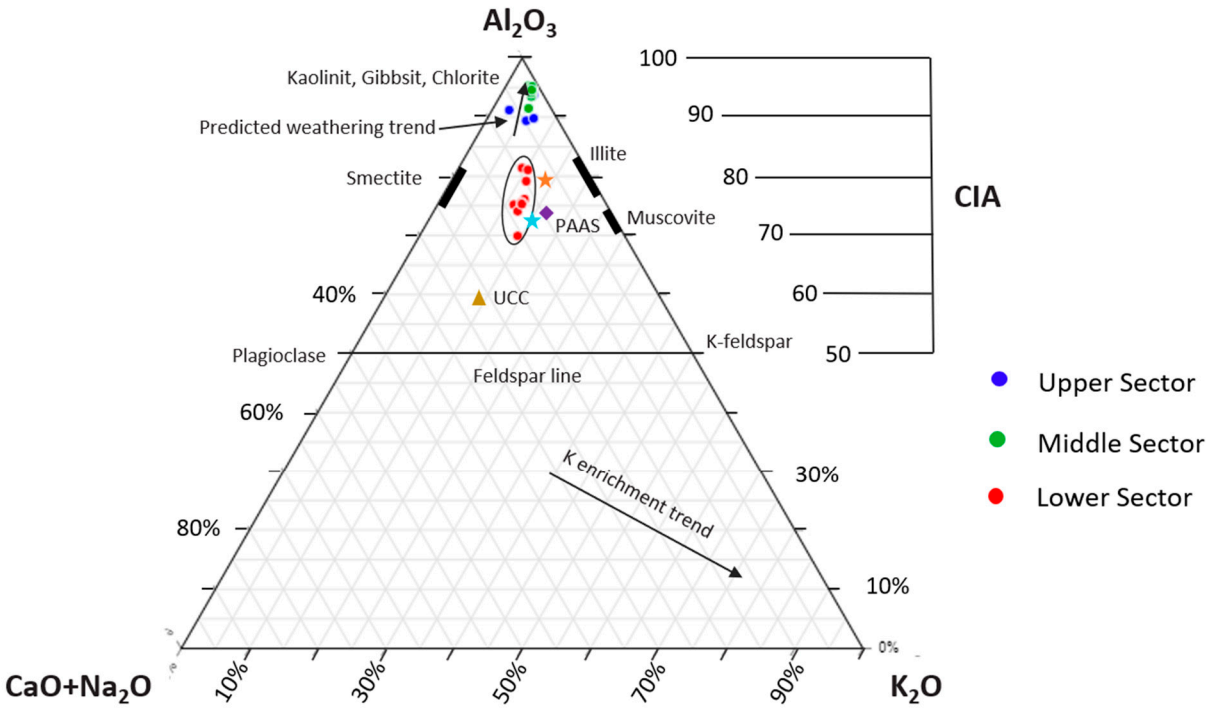

Figure 7. A-CN-K ternary diagram (Fedo et al., 1995 [31]; Nesbit and Young 1982 [30]) showing the influence of weathering on sediment compositional history. The blue star represents the bottom sediments of the Amazon River downstream from Santarém (about 230 km upstream from the mouth of the Xingu River) obtained by Medeiros Filho et al., 2016 [20], and the yellow stars represent data from suspended material essentially from the Xingu River by Baturin, 2019 [16].

In general, chemical weathering in tributaries exhibits more diversity than in the main flow, particularly when considering the CIA. Smaller tributary basins display greater local variation [42,43]. The CIA allows for the assessment of the intensity of chemical weathering, but it can also be seen in conjunction with the mineralogical maturity of the sediments. This is important because more immature sediments, with a greater presence of feldspars and easily weatherable minerals (such as smectite), indicate less exposure to weathering and less prolonged transport. On the other hand, the predominance of quartz and more resistant minerals reflects more mature sediments, which have undergone greater reworking and weathering.

4.3. Conservation of Trace Elements and REE

The composition of trace elements in river sediments results from the interplay of various factors, including provenance, weathering, diagenesis, sediment sorting, and the aqueous geochemistry of individual elements [35]. Zirconium is particularly valuable for provenance characterization due to its low solubility, relative immobility, and transport as terrigenous components. Zirconium showed a specific correlation with Th, with restricted heavy mineral enrichment, whereas high Zr contents were mainly attributed to zircon and possibly rutile content. Quartz, being a more abundant and resistant mineral, generally does not significantly influence the concentration of zirconium in sediments. However, its presence as a dominant component in sediments can affect the fraction of heavy minerals and, therefore, indirectly influence the concentration of zirconium (Figure 8).

Elemental geochemistry facilitates the tracing of sediment and sedimentary rock provenance. This is achieved by analyzing immobile elements (Al, Ti, Zr, Hf, and Th) and rare earth elements (REEs), which are less fractionated during weathering processes and tend to concentrate in bottom sediments, as opposed to the dissolved fraction in rivers [43,44].

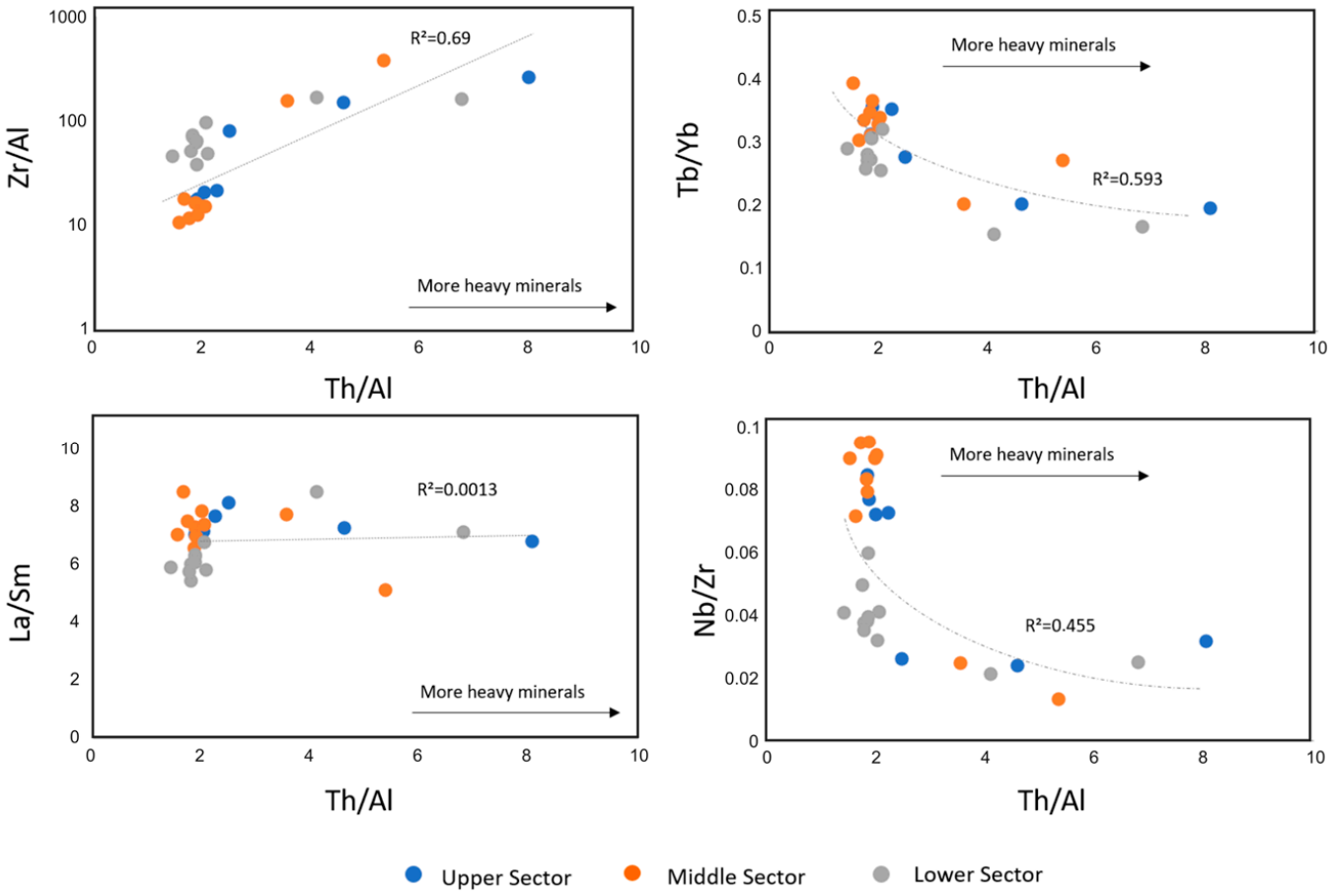

Figure 8. Conservative ratios of trace elements associated with Th/Al ratio discriminated among sectors.

The La/Sm ratio indicated some fractionation of REEs, showing a higher enrichment of light REEs (LREE) in Xingu River samples. REE fractionation in Amazon River sediments has been previously observed by Goldstein and Jacobsen (1988) [45], which exhibited patterns of heavy REE (HREE) depletion.

The chemistry of riverbed sediments often does not accurately reflect their source rocks after weathering [32]. However, REE abundance and patterns have been reasonably well preserved during weathering, reflecting their relatively immobile nature during sedimentary and hydrological processes.

In summary, REE mobility and fractionation may or may not have a direct relationship with chemical weathering. Although the REE composition of river sediments may differ from the source regions (weathering profile), it may not be widely indicative of total weathering processes. Fine river sediments reflect the average of weathered crust in river basins and tend to exhibit uniform REE patterns normalized by the Upper Continental Crust (UCC) [46]. Therefore, sediments in large rivers, despite their different catchment sizes and geological provenance, may all represent the average terrigenous matter delivered to the ocean in terms of REE compositions.

Once again, the relative enrichment of LREE in the samples, compared to HREE, indicates predominantly felsic sources. The relative abundance of source rocks, weathering conditions in the source regions, and hydraulic sorting processes are considered the main controlling factors of REE contents in sediments [45].

Previous studies have emphasized the pH condition as an important control factor and suggested that REEs are easily removed from clays under acidic conditions (weathering) but become stable under neutral or alkaline conditions (erosion and transport). According to the diagram proposed by Su et al., 2019 [47], sediment samples tend to align with

a profile more associated with river transport and erosion (Figure 9), as shown by the $LREE/HREE_{UCC}$ ratio (normalized to the Upper Continental Crust). The $LREE/HREE_{UCC}$ ratios predominantly showed values below 1 in the Lower sector and above 1 in the Middle and Upper sectors.

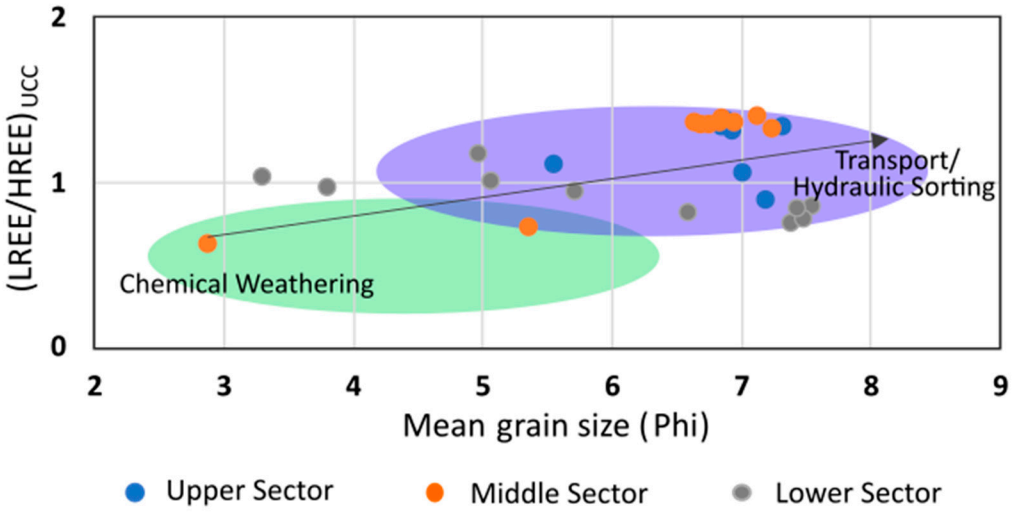

Figure 9. The LREE/HREEUCC ratio and average particle size (phi scale) distribution have been demonstrated to distinguish chemical weathering from transport/hydraulic categorization. The black arrow indicates the transition between predominance of weathering and remobilization of sediments by hydraulic transport. (adapted from Su et al. in 2019 [47]).

REE fractionation in siliciclastic sediments is primarily controlled by the degree of chemical weathering, while river processes (i.e., hydraulic sorting) can homogenize weathering, thereby weakening REE fractionation in river sediments. In other words, mineral partitioning induced by hydraulic sorting further controls REE composition by altering the proportion of fine-grained REE components [47].

This trade-off between weathering and river movement is reinforced by the $LREE/HREE_{UCC}$/Phi relationship. Clays and other fine sediments typically develop in conditions characterized by a predominance of chemical weathering and low transport energy; consequently, REE fractionation appears to be more effective in evaluating chemical degradation in environments that are less dynamic (lentic). Coarser sediments, such as sands, are commonly linked to ecosystems with higher energy, characterized by more efficient movement and less significant chemical weathering conditions.

Dynamic sediments are characterized by continuous movement caused by substantial hydrodynamic forces. Lower sector units are generally less susceptible to chemical weathering. The continuous process of reworking and migration poses challenges for minerals to undergo chemical modification, as the grains are frequently excluded from settings where chemical weathering would be more efficient. This phenomenon can be attributed to the inherent dynamics of the Xingu River and the seasonal cycle of the Amazon River, with the potential exacerbation of this situation by tidal effects.

4.4. Provenance and Geochemical Assignment of Sediments

The Amazon River Basin is distinguished by vigorous dynamics of water flow and rapid deposition of sediment, mostly consisting of Phanerozoic layers. The continuous movements of rivers can lead to the intermixing of sediments originating from many sources. The existence of younger Phanerozoic depositions indicates that the process of weathering may be comparatively less severe in comparison to older, more extensively weathered regions. The assemblage of sediments originating from many sources can increase the complexity of interpretation, yet the existence of primary minerals may suggest a reduced degree of weathering.

The geology in the Xingu Basin is well-preserved, mostly consisting of crystalline shields originating from Central Brazil (Precambrian terranes). These regions consist of older, less modified rocks. Precambrian terranes typically have a more extensive and intricate weathering history, leading to more significant chemical composition changes. The vast and dynamic flow of water in the Amazon Basin can lead to the formation of sediments that reflect a combination of many origins and phases of weathering. In the Xingu Basin, the well-preserved and ancient geology can result in sediments that exhibit more distinct indications of deep weathering and their genesis in ancient rocks.

In general, a geochemical pattern of element mobility, whether by enrichment or depletion of major and trace elements, is expected. Considering that the study area represents only a small stretch of a river nearly 1000 km in length, investigating its lower course to its mouth refines the geochemical balance, in addition to the significant contribution from the river receiving its discharge. Considering physical variables such as river discharge and tides, these effects may be further enhanced. A schematic model for the Xingu River, considering the ria extent, a small upstream section, and the downstream section to the mouth of the Amazon River regarding geochemical mobility, is presented in Figure 10.

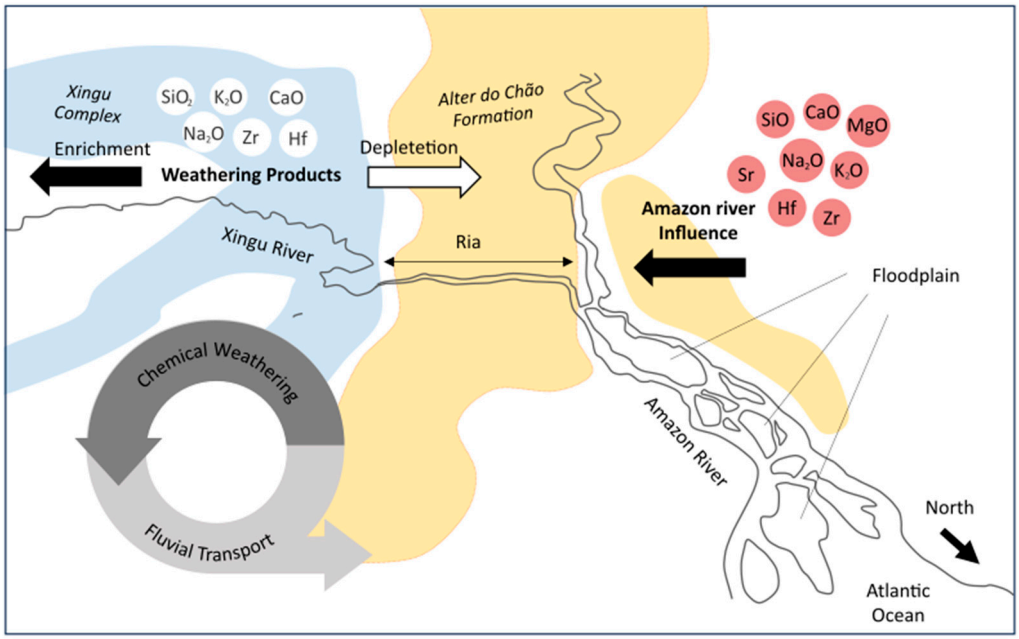

Figure 10. Schematic model of enrichment and depletion of elements in the Xingu River and the influence of the Amazon River on geochemical balance. The domains in blue represent the Xingu complex of the Archean age, and the yellow is the Alter do Chão formation of the Cenozoic age.

Depletion patterns of elements such as SiO_2, K_2O, CaO, Na_2O, Zr, and Hf are expected for river transport, considering the presence of secondary minerals in the Lower sector and the dissolution of silica and potassium in primary minerals. However, the influence of the Amazon River, possibly associated with seasonal hydrology, reshapes the geochemistry in its lower course, as well as textural and mineralogical patterns for nearly one-third of the ria, encompassing its contribution to almost, if not the entire, Lower sector.

5. Conclusions

The downstream section of the Xingu ria (Lower sector) was distinguished from the main channel and the upstream section (Middle and Upper sector), indicating the presence of non-exclusive sources other than the Xingu River itself. There may be sediment input from the Amazon River in this location towards the confluence sector or even material exchange at the Xingu-Amazonas confluence, highlighting mixing patterns.

The assessment of chemical weathering and river transport in the geochemical composition of Xingu ria sediments indicated a depletion of elements such as SiO_2, K_2O,

CaO, Na_2O, Zr, and Hf. There was an alignment between the Chemical Alteration Index (CIA) and ΣREE, with LREE enrichment, a pattern already established by Amazon River tributaries.

A connection was seen between the mobility of major and trace elements and the zonation of the ria, resembling that of estuaries. Specifically, the bottom sector exhibited a more distinct differentiation from the Middle and Upper sectors. The REEs demonstrated relative preservation in their concentrations due to the action of chemical weathering and river transport from upstream to downstream.

The sediments in the main channel of the Xingu ria provide insights into geology and fluvial sediment transport and have much to reveal about the material drained from a drainage basin. The evaluated data allowed for the development of models for the depletion and enrichment of less conservative elements, hydrological processes, and the geochemical balance.

The zoning pattern observed through granulometry, along with associated mineralogy and geochemistry, corroborated with multivariate statistics (PCA) to confirm the formation of well-individualized groups between the upstream sector (Upper and Middle) and the downstream sector of the ria (lower). There were also clear indications of sediments originating from the ria's banks, possibly a product of erosion from adjacent regions.

An analysis of geochemical indicators derived from basic ratios proved to be successful in determining the origin of sediments. Hence, the most effective approach was to analyze the movement, transportation, and accumulation of sediment in the Xingu River using geochemical indicators and mineralogical analysis. The lower section of the Amazon River serves as both the source and sink of several amounts of depositional material. Consequently, the presence of several events clearly indicates the impact of the Amazon River on the sediments of the lower Xingu.

The geochemistry of bottom sediments in the lower Xingu River, despite draining the cratonic regions in higher elevations, reaffirms that the bedload is derived from heterogeneous sources with predominantly intermediate igneous compositions and has undergone significant recycling during river transport.

Supplementary Materials: The following supporting information can be downloaded at: https://www.mdpi.com/article/10.3390/min14111101/s1, Table S1: Concentrations of trace elements analyzed for the sediments with opening by fusion with lithium metaborate and reading by ICP-MS; Table S2: Correlation matrix between the analyzed elements; Table S3: Factor analysis in addition to PCA analysis.

Author Contributions: Conceptualization, L.C.M.F. and N.E.A.; methodology, L.C.M.F. and J.M.L.; formal analysis, L.C.M.F.; investigation, N.E.A.; resources, N.E.A.; data curation, L.C.M.F. and J.M.L.; writing—original draft preparation, L.C.M.F. and T.P.S.; writing—review and editing, J.M.L.; J.F.B. and G.N.S.; visualization, L.C.M.F.; supervision, J.M.L., J.F.B. and G.N.S.; project administration, N.E.A.; funding acquisition, N.E.A. All authors have read and agreed to the published version of the manuscript.

Funding: The research received some funding from the Coordenação de Aperfeiçoamento de Pessoal de Nível Superior-Brasil (CAPES)–Pró-Amazônia Program, approved under Finance Code 3290/2013.

Data Availability Statement: The geochemical data of this work are available in Supplementary Materials. Any additional data about the project, including granulometry and mineralogical data, can be found at http://repositorio.ufpa.br:8080/bitstream/2011/14581/1/Tese_HidrodinamicaTransporteProveniencia.pdf (accessed on 21 January 2024).

Acknowledgments: Thanks are extended to the Conselho Nacional de Desenvolvimento Científico e Tecnológico–CNPQ for providing the doctoral and research funding to the authors. In the CNPq research, Nils E. Asp assumed the role of research project coordinator.

Conflicts of Interest: The authors declare no conflicts of interest.

References

1. Gaillardet, J.; Dupré, B.; Louvat, P.; Allègre, C. Global silicate weathering and CO_2 consumption rates deduced from the chemistry of large rivers. *Chem. Geol.* **1999**, *159*, 3–30. [CrossRef]
2. Singh, S.K.; France-Lanord, C. Tracing the distribution of erosion in the Brahmaputra watershed from isotopic compositions of stream sediments. *Earth Planet. Sci. Lett.* **2002**, *202*, 645–662. [CrossRef]
3. Tripathi, J.K.; Ghazanfari, P.; Rajamani, V.; Tandon, S. Geochemistry of sediments of the Ganges alluvial plains: Evidence of large-scale sediment recycling. *Quat. Int.* **2007**, *159*, 119–130. [CrossRef]
4. Hossain, H.Z.; Kawahata, H.; Roser, B.P.; Sampei, Y.; Manaka, T.; Otani, S. Geochemical characteristics of modern river sediments in Myanmar and Thailand: Implications for provenance and weathering. *Chem. Erde* **2017**, *77*, 443–458. [CrossRef]
5. Natali, C.; Bianchini, G. Geochemical proxies of sediment provenance in alluvial plains with interfering fluvial systems: A study case from NE Italy. *Catena* **2017**, *157*, 67–74. [CrossRef]
6. Maharana, C.; Srivastava, D.; Tripathi, J.K. Geochemistry of sediments of the Peninsular rivers of the Ganga basin and its implication to weathering, sedimentary processes and provenance. *Chem. Geol.* **2018**, *483*, 1–20. [CrossRef]
7. Chen, J.; Liu, P.; Sun, D.; Zhang, D.; Miao, B.; Chen, J. Riverine Sediment Geochemistry as Provenance Fingerprints along the Eastern Coast of China: Constraint, Approach, and Application. *Minerals* **2020**, *10*, 29. [CrossRef]
8. Irion, G.; Kalliola, R. Long-term landscape development processes in Amazonia. In *Amazonia, Landscape and Species Evolution: A Look into the Past*; Hoorn, C.M., Wesselingh, F.P., Eds.; John Wiley & Sons: New York, NY, USA, 2010; pp. 185–197.
9. Albert, J.S.; Val, P.; Hoorn, C. The changing course of the Amazon River in the Neogene: Center stage for Neotropical diversification. *Neotropical Ichthyol.* **2018**, *16*, 1–24. [CrossRef]
10. Bertassoli, D.J.; Sawakuchi, A.O.; Sawakuchi, H.O.; Pupim, F.N.; Hartmann, G.A.; McGlue, M.M.; Chiessi, C.M.; Zabel, M.; Schefuß, E.; Pereira, T.S.; et al. The Fate of Carbon in Sediments of the Xingu and Tapajós Clearwater Rivers, Eastern Amazon. *Front. Mar. Sci.* **2017**, *4*, 44. [CrossRef]
11. Fricke, A.T.; Nittrouer, C.A.; Ogston, A.S.; Nowacki, D.J.; Asp, N.E.; Filho, P.W.M.S.; da Silva, M.S.; Jalowska, A.M. River tributaries as sediment sinks: Processes operating where the Tapajós and Xingu rivers meet the Amazon tidal river. *Sedimentology* **2017**, *64*, 1731–1753. [CrossRef]
12. Silva, A.M.; Asp, N.E.; Gomes, V.J.; Braga, A.A.; Gomes, J.D.; Fricke, A.T.; Souza-Filho, P.W.M.; Souza, T.P.; Almeida, P.D.; Ogston, A.S.; et al. Recent sedimentation in an Amazon tidal tributary: Integrated analysis of morphology and sedimentology. *J. South Am. Earth Sci.* **2021**, *107*, 103134. [CrossRef]
13. Martinelli, L.A.; Victoria, R.L.; Dematte, J.L.I.; Richey, J.; Devol, A. Chemical and mineralogical composition of Amazon River floodplain sediments, Brazil. *Appl. Geochem.* **1993**, *8*, 391–402. [CrossRef]
14. Gaillardet, J.; Dupre, B.; Allegre, C.J.; Négrel, P. Chemical and physical denudation in the Amazonian River Basin. *Chem. Geol.* **1997**, *142*, 141–173. [CrossRef]
15. Horbe, A.M.C.; da Trindade, I.R.; Dantas, E.L.; Santos, R.V.; Roddaz, M. Provenance of quaternary and modern alluvial deposits of the Amazonian floodplain (Brazil) inferred from major and trace elements and Pb–Nd–Sr isotopes. *Palaeogeogr. Palaeoclim. Palaeoecol.* **2014**, *411*, 144–154. [CrossRef]
16. Baturin, G.N.; Gordeev, V.V. Geochemistry of Suspended Matter in the Amazon River Waters. *Geochem. Int.* **2019**, *57*, 197–205. [CrossRef]
17. Vital, H.; Stattegger, K. Lowermost Amazon River: Evidence of late Quaternary sea-level fluctuations in a complex hydrodynamic system. *Quat. Int.* **2000**, *72*, 53–60. [CrossRef]
18. Seyler, P.T.; Boaventura, G.R. Distribution and partition of trace metals in the Amazon basin. *Hydrol. Process.* **2003**, *17*, 1345–1361. [CrossRef]
19. Bouchez, J.; Gaillardet, J.; France-Lanord, C.; Maurice, L.; Dutra-Maia, P. Grain size control of river suspended sediment geochemistry: Clues from Amazon River depth profiles. *Geochem. Geophys. Geosystems* **2011**, *12*, Q03008. [CrossRef]
20. Filho, L.C.M.; Lafon, J.-M.; Filho, P.W.M.S. Pb Sr Nd isotopic tracing of the influence of the Amazon River on the bottom sediments in the lower Tapajós River. *J. S. Am. Earth Sci.* **2016**, *70*, 36–48. [CrossRef]
21. Irion, G. Sedimentation and sediments of Amazonian rivers and evolution of the Amazonian landscape since Pliocene times. In *The Amazon*; Sioli, H., Ed.; Monographiae Biologicae; Springer: Dordrecht, The Netherlands, 1984; Volume 56. [CrossRef]
22. Ahmad, I.; Chandra, R. Geochemistry of loess-paleosol sediments of Kashmir Valley, India: Provenance and weathering. *J. Asian Earth Sci.* **2013**, *66*, 73–89. [CrossRef]
23. Garzanti, E.; Resentini, A. Provenance control on chemical indices of weathering (Taiwan river sands). *Sediment. Geol.* **2016**, *336*, 81–95. [CrossRef]
24. Vasquez, M.L.; Rosa-Costa, L.T. (org.). Geologia e Recursos Minerais do Estado do Pará: Texto Explicativo do Mapa Geológico e de Recursos Minerais do Estado do Pará. Belém, PA: CPRM, 2008. 327 p. il. Color. Programa Geologia do Brasil (PGE), Integração, Atualização e Difusão de Dados da Geologia do Brasil. Mapas Geológicos Estaduais. Escala 1:1.000,000. Available online: https://rigeo.sgb.gov.br/handle/doc/10443 (accessed on 21 January 2024).
25. Kroonenberg, S.B.; de Roever, E.W.F. Geological Evolution of the Amazonian Craton. In *Amazonia: Landscape and Species Evolution: A Look into the Past*; Hoorn, C., Wesselingh, F.P., Eds.; John Wiley & Sons, Inc.: Hoboken, NJ, USA; pp. 7–19. [CrossRef]

26. Hoorn, C.; Roddaz, M.; Dino, R.; Soares, E.; Uba, C.; Ochoa-Lozano, D.; Mapes, R. The Amazonian Craton and its influence on past fluvial systems (Mesozoic-Cenozoic, Amazonia). In *Amazonia: Landscape and Species Evolution—A Look into the Past*; Hoorn, C., Wesselingh, F.P., Eds.; Blackwell. Publishing Ltd.: West Sussex, UK, 2010; pp. 103–122. [CrossRef]
27. Tassinari, C.C.; Macambira, M.J. Geochronological provinces of the Amazonian Craton. *Episodes* **1999**, *22*, 174–182. [CrossRef] [PubMed]
28. Tassinari, C.C.G.; Macambira, M.J.B. A evolução tectônica do Cráton Amazônico. In *Geologia do Continente Sul-Americano: Evoluçao da Obra de Fernando Flávio Marques de Almeida*; Recuperado de Beca: São Paulo, Brazil, 2004. Available online: https://repositorio.usp.br/directbitstream/92ee8375-3d03-4514-a8a9-98c7d6eaba02/1417504.pdf (accessed on 30 January 2021).
29. Folk, R.L.; Ward, W. Brazos river bar: A study in the significance of grain-size parameters. *J. Sediment. Res.* **1957**, *27*, 3–26. [CrossRef]
30. Nesbitt, H.W.; Young, G.M. Early Proterozoic climates and plate motions inferred from major chemistry of lutites. *Nature* **1982**, *299*, 715–717. [CrossRef]
31. Fedo, C.M.; Nesbitt, H.W.; Young, G.M. Unraveling the effects of potassium metasomatism in sedimentary rocks and paleosols, with implications for paleo-weathering conditions and provenance. *Geology* **1995**, *23*, 921–924. [CrossRef]
32. Nesbitt, H.W.; Young, G.M.; McLennan, S.M.; Keays, R.R. Effects of chemical weathering and sorting on the petrogenesis of siliciclastic sediments, with implication for provenance studies. *J. Geol.* **1996**, *104*, 525–542. [CrossRef]
33. Mineli, R.C. Proveniência e Retrabalhamento Sedimentar das Areias da Volta Grande do rio Xingu, PA. MS Dissertation, Instituto de Geociências, Universidade de São Paulo, Belém, Portugal, 2013; p. 74. Available online: http://www.teses.usp.br/teses/disponiveis/44/44141/tde-07042014-093930/ (accessed on 21 May 2021).
34. Souza, T.P. 2018. Influência do rio Amazonas nos sedimentos de fundo do rio Xingu: Evidências mineralógicas e geoquímicas. MS Dissertation, Instituto de Geociências, Universidade Federal do Pará, Belém, p. 115. Available online: https://repositorio.ufpa.br/jspui/handle/2011/11701 (accessed on 5 June 2021).
35. Rollinson, H. Using trace elements data. In *Using Geochemical Data: Evaluation, Presentation, Interpretation*, 1st ed.; Rollinson, H., Ed.; Routledge: London, UK, 1993; pp. 133–134. [CrossRef]
36. Singh, M.; Sharma, M.; Tobschall, H.J. Weathering of the Ganga alluvial plain, northern India: Implications from fluvial geochemistry of the Gomati River. *Appl. Geochem.* **2005**, *20*, 1–21. [CrossRef]
37. Hu, D.; Böning, P.; Köhler, C.M.; Hillier, S.; Pressling, N.; Wan, S.; Brumsack, H.J.; Clift, P.D. Deep sea records of the continental weathering and erosion response to East Asian monsoon intensification since 14 ka in the South China Sea. *Chem. Geol.* **2012**, *326–327*, 1–18. [CrossRef]
38. K, B. Geochemical characteristics of sandstones from Cretaceous Garudamangalam area of Ariyalur, Tamilnadu, India: Implications of provenance and tectonic setting. *J. Earth Syst. Sci.* **2017**, *126*, 45. [CrossRef]
39. Sahoo, P.K.; Guimarães, J.T.F.; Souza-Filho, P.W.M.; da Silva, M.S.; Nascimento, W.; Powell, M.A.; Reis, L.S.; Pessenda, L.C.R.; Rodrigues, T.M.; da Silva, D.F.; et al. Geochemical characterization of the largest upland lake of the Brazilian Amazonia: Impact of provenance and processes. *J. S. Am. Earth Sci.* **2017**, *80*, 541–558. [CrossRef]
40. Roser, B.P.; Korsch, R.J. Plate Tectonics and Geochemical Composition of Sandstones: A Discussion. *J. Geol.* **1985**, *93*, 81–84. [CrossRef]
41. McLennan, S.M. Weathering and Global Denudation. *J. Geol.* **1993**, *101*, 295–303. [CrossRef]
42. Silva, M.M.V.G.; Pinto, M.M.C.; Carvalho, P.C.S. Major, trace and REE geochemistry of recent sediments from lower Catumbela River (Angola). *J. Afr. Earth Sci.* **2016**, *115*, 203–217. [CrossRef]
43. He, M.; Zheng, H.; Clift, P.D.; Tada, R.; Wu, W.; Luo, C. Geochemistry of fine-grained sediments in the Yangtze River and the implications for provenance and chemical weathering in East Asia. *Prog. Earth Planet. Sci.* **2015**, *2*, 32. [CrossRef]
44. Bhatia, M.R. Rare earth element geochemistry of Australian Paleozoic graywackes and mudrocks: Provenance and tectonic control. *Sediment. Geol.* **1985**, *45*, 97–113. [CrossRef]
45. Goldstein, S.J.; Jacobsen, S.B. Rare earth elements in river waters. *Earth Planet. Sci. Lett.* **1988**, *89*, 35–47. [CrossRef]
46. Taylor, S.R.; McLennan, S.M. The Continental Crust: Its composition and evolution: Oxford, Blackwell, 311 p. ISBN 0 632 01148 3. *Geol. Mag.* **1985**, *122*, 673–674. [CrossRef]
47. Su, N.; Yang, S.; Guo, Y.; Yue, W.; Wang, X.; Yin, P.; Huang, X. Revisit of rare earth element fractionation during chemical weathering and river sediment transport. *Geochem. Geophys. Geosyst.* **2017**, *18*, 935–955. [CrossRef]